Journal of the Korean Society
for Nondestructive Testing
Vol. 28, No. 3 (2008. 6)

SAFT Based Imaging and Centroid Technique for Classification of UT Signals from the Steam Generator of a Nuclear Power Plant

Daewon Kim

Abstract Many technical methods are used for nondestructive testing field for solid materials. Among those, ultrasonic inspection methods are widely used and one of the popular methods involves the extraction of an appropriate set of features followed by the use of a neural network for the classification of the signals in the feature space. This paper describes an approach which uses LMS method to determine the coordinates of the ultrasonic probe followed by the use of SAFT with centroid technique to estimate the location of the ultrasonic reflector. The method is employed for classifying UT-NDE signals from the steam generator tubes in a nuclear power plant. The classification results are presented for the ultrasonic signals from cracks and deposits within steam generator tubes.

Keywords: SAFT, Centroid , Ultrasonic NDE, Classification, LMS

1. Introduction

Ultrasonic inspections are widely used for the flaw detection of materials. The signal analysis step plays a crucial part in the data interpretation process. A number of signal processing methods have been proposed to classify ultrasonic flaw signals. The ultrasonic inspections are common tool in the nondestructive evaluation (NDE) of the steam generator tubes in nuclear power plants (Khan, 2001). In order to evaluate the structural status of a material, many researchers have proposed various kinds of methods which could classify quantitatively ultrasonic flaw signals. Those methods are mainly based on the signal analysis and an automatic signal classification schemes which have the potential to provide reasonable interpretation of inspection data. One of the popular approaches to perform a classification of ultrasonic signals involves the extraction of features from data followed by the use of a neural network based schemes such as a multi-layer perceptron neural network with back-propagation learning algorithm (Khan, 2001; Polikar et al., 1998) and genetic algorithm (Du-Yih, 1998). The classification of ultrasonic signals also can be done alternatively by applying deconvolution approach (Demirli and saniie, 2001; Taxt, 2001). In this paper, we approached the ultrasonic signals' classification problem from a geometrical point of view and a least mean square (LMS) algorithm to estimate the parameters which are used in conjunction with synthetic aperture focusing technique (SAFT) followed by centroid method. The main objective is to develop a method for discriminating crack signals from those due to deposits. Several issues need to be studied to achieve this objective. Firstly, investigation of the characteristics of the collected ultrasonic

Received: February 1, 2008, Revised: May 17, 2008, Accepted: May 20, 2008, Department of Multimedia Engineering, Division of Computer Engineering, Dankook University, San 29, Anseodong, Cheonan, Chungnam, 330-714, Republic of Korea, (E-mail: drdwkim@dku.edu)

signals should be done. Secondly, a coordinate system for the probe and the tube should be developed to produce a basis for estimating the location of the probe inside the tube. Thirdly, a technique for estimating the coordinates and its canting angle of the probe should be developed. Fourthly, we need to image the geometry of the scatterers using SAFT with centroid and the technique requires reasonably accurate estimates of the location of the probe relative to the tube wall and other scatterers. Finally, the classification of the scatterer either as a crack or a deposit should be performed using its centroid.

2. UT NDE for Steam Generator Tubes

Steam generators are used for converting water into steam by heat produced in the reactor core in a nuclear power plant. Each steam generator contains approximately 3,000 to 16,000 tubes through which hot radioactive water flows. The thermal energy transferred from the primary coolant causes the generation of steam which in turn is used for operating turbines. The tubes have to be inspected periodically to ensure that the tubes are not causing nuclear contamination of the water on the secondary side. A popular inspection technique involves the use of ultrasonic NDE methods. In inspecting the steam generator tubes, the ultrasonic transducer moves along the tube axis with water sealed between the tube wall and the transducer. Fig. 1 shows the ultrasonic inspection setup. This figure illustrates the tube is in the region contacting with a surrounding structure called as *tube sheet* which is the black triangle shaped geometry on both sides of the tube. There is a possibility that the tubes have cracks outside the wall in this region. Such cracks usually extend 2 inches along the tube within and above the *tube sheet* support. Additionally, chemical precipitates and dissolved metallic compounds are deposited on the *tube sheet* in this region.

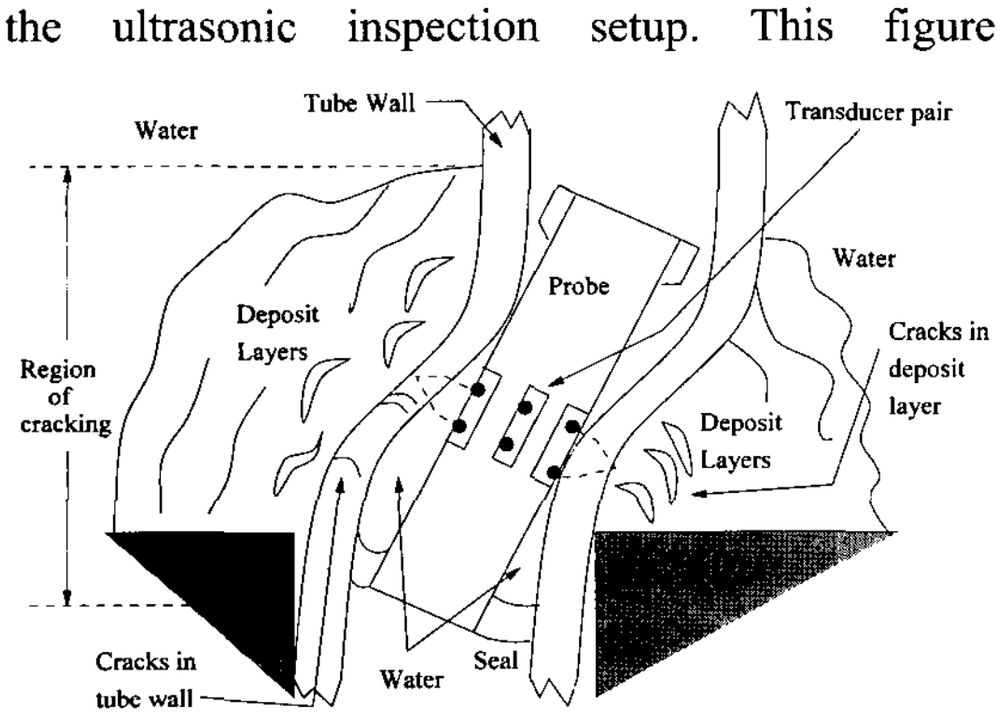

Fig. 1 Geometry of ultrasonic NDE of the steam generator tube

The transducer has nominal center frequencies of 8-11 MHz (within 6 dB from ~6 to ~16 MHz). The sampling frequency is 80 MHz and the thickness of the tube wall is 0.047 inches. The ultrasonic transducer transmits longitudinal waves with a 19.5° incident angle. The wave travels through the water and is incident on the inner wall of the tube. When the wave arrives at the tube inner wall, mode conversion occurs and the shear wave travels into the tube wall internally at a 45° refraction angle. Signals generated by the piezoelectric elements are sampled using an 8 bit converter. The sampled and digitized signal is a 482-point signal displayed in an A-scan format. The ultrasonic wave can be scattered by cracks present in the tube or inhomogeneities present in the chemical precipitates and dissolved metallic compounds that are deposited outside. The signals from cracks must be discriminated from those due to deposits, since cracks in the tube wall may result in leakage of the primary coolant. The signals from deposits are ignorable indications and are not sources of concern. Consequently there is considerable interest in automatic methods for analyzing the data.

3. Distance Computation for the Probe and the Tube

3.1 Coordinates Location using Geometric Approach

The transducers are arrayed in two tiers and

spaced 45° apart on the circumference. We call the eight transducers in a tier as constituting a set. There are a total of six sets. A pair of these sets correspond to one set of forward and reverse looking elements. The probe moves forward axially along the tube axis during the inspection. Since the probe ID is less than the inner diameter of the tube and the probe axis may not be aligned with the tube axis. The offset in coordinates and the canting angle with respect to the tube axis needs to be estimated. In order to do that, we can begin by using an appropriate coordinate system. Fig. 2 displays the spherical and a cylindrical coordinate system where r is a distance from the center of one set of transducers to one transducer, R is a radius of the cylinder, θ is an angle between the Z-axis and the point T, ϕ is a rotation angle of T with respect to the Z-axis, T is a location of one transducer, and P is a straight point on the cylinder from T. The Z-axis, in both cases, is aligned along the tube axis while the X-Y plane corresponds to the circumferential cross section of the tube.

We assume that one set of transducers can cant inside the cylinder with the center of the probe cross section located at (X=0, Y=0). Focusing on the spherical coordinate system, if T represents the location of one transducer in a set, the X, Y, Z coordinates are given by (Hayt, 1989),

$$X_T = r\sin\theta\cos\phi \tag{1}$$

$$Y_T = r\sin\theta\sin\phi \tag{2}$$

$$Z_T = r\cos\theta \tag{3}$$

The next step involves estimation of the coordinates of the remaining seven transducers in the set. We do so by defining the following terms in Fig. 3 where $\mathbf{N_T}$ is a normal to the one set of transducers' circumferential cross section surface, $\mathbf{T_i}$ is a vector of i_{th} transducer, ρ_i is an angle between $\mathbf{T_i}$ and $\mathbf{T_1}$ (i=1,2,.....,8).
Then the normal to the surface containing the eight sensors can be determined using

$$\mathbf{N_T} = -\cos\theta\cos\phi\mathbf{a}_x - \cos\theta\sin\phi\mathbf{a}_y + \sin\theta\mathbf{a}_z \tag{4}$$

and $\mathbf{T_1}$ can be derived from eqns. (1) through (3) as

$$\mathbf{T_1} = r\sin\theta\cos\phi\mathbf{a}_x + r\sin\theta\sin\phi\mathbf{a}_y + r\cos\theta\mathbf{a}_z \tag{5}$$

and $\mathbf{T_2}$ through $\mathbf{T_4}$ can be calculated as

$$\begin{aligned}\mathbf{T_2} = {} & r\left(\cos 45^\circ\sin\theta\cos\phi - \sin 45^\circ\sin\phi\right)\mathbf{a}_x \\ & + r\left(\cos 45^\circ\sin\theta\sin\phi + \sin 45^\circ\cos\phi\right)\mathbf{a}_y \\ & + r\cos 45^\circ\cos\theta\mathbf{a}_z\end{aligned} \tag{6}$$

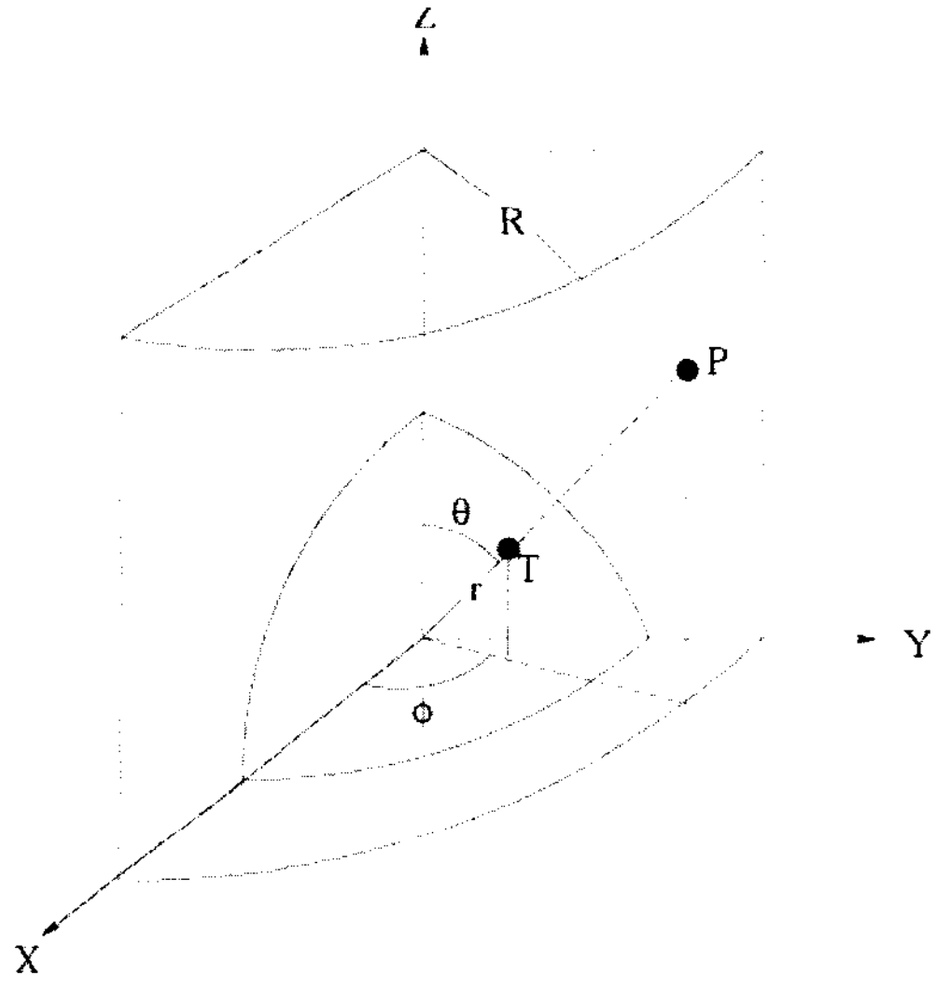

Fig. 2 Spherical and cylindrical coordinate systems for the probe and the tube

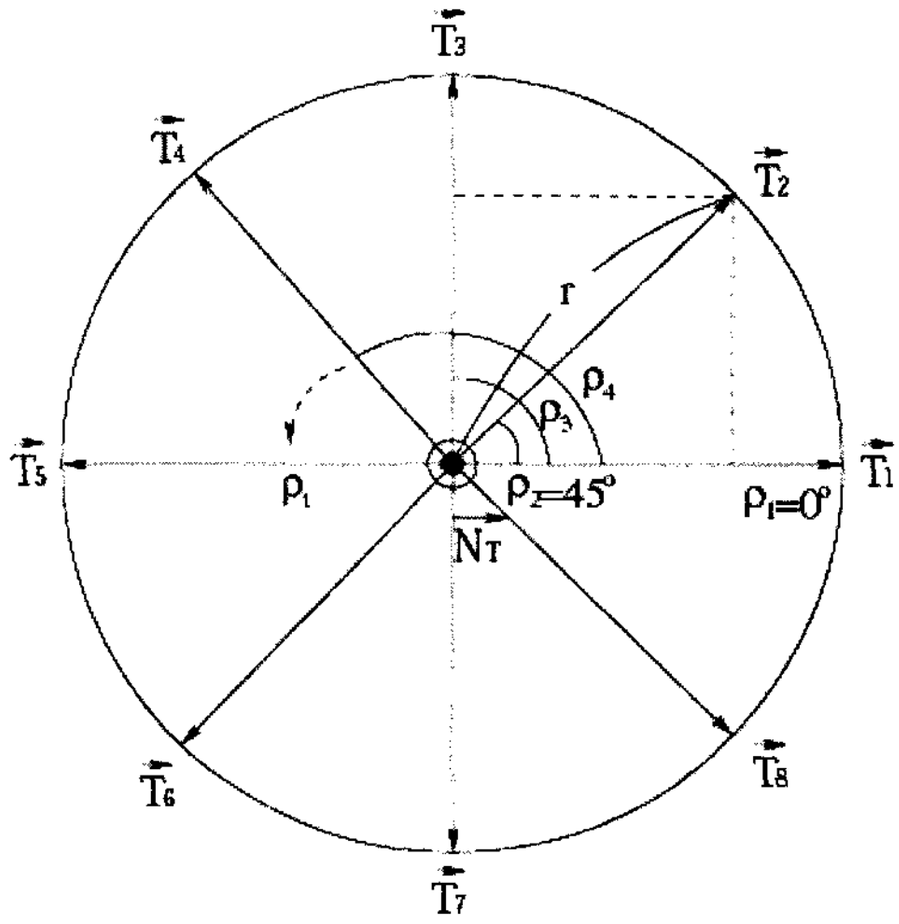

Fig. 3 Coordinates of one set of transducers

$$\mathbf{T}_3 = -r\sin 90^\circ \sin\phi \mathbf{a}_x + r\sin 90^\circ \cos\phi \mathbf{a}_y \quad (7)$$

$$\begin{aligned}\mathbf{T}_4 = {} & r\left(\cos 135^\circ \sin\theta\cos\phi - \sin 135^\circ \sin\phi\right)\mathbf{a}_x \\ & + r\left(\cos 135^\circ \sin\theta\sin\phi + \sin 135^\circ \cos\phi\right)\mathbf{a}_y \\ & + r\cos 135^\circ \cos\theta \mathbf{a}_z\end{aligned} \quad (8)$$

In order to obtain the coordinates of the remaining points which are $\mathbf{T_5}$, $\mathbf{T_6}$, $\mathbf{T_7}$ and $\mathbf{T_8}$, we can multiply the X,Y and Z coordinate values of $\mathbf{T_1}$, $\mathbf{T_2}$, $\mathbf{T_3}$ and $\mathbf{T_4}$ by -1 respectively since those four vectors are symmetrical to each other through the center point, (0,0,0). However, as we mentioned at the beginning of this section, the spherical coordinates of the eight sensors can be shifted towards any direction along the X-, Y- and Z-axis. To generalize movement of the coordinates within the tube, the translation, C_x, C_y and C_z of the X, Y and Z coordinate values should be summed with all eight vectors appropriately. The translations mean the movement offsets of the probe inside the tube for each X, Y and Z directions. The tube can be considered as a cylinder as shown in Fig. 2. We assume that the center is fixed at (0,0,0) for the two coordinate systems. Then, the X, Y, Z coordinates of a point P on the cylinder can be obtained as follows

$$X_P = R\cos\phi \quad (9)$$

$$Y_P = R\sin\phi \quad (10)$$

$$Z_P = R\cos\theta \quad (11)$$

The θ and ϕ in the above equations can be transformed and represented in terms of X_T, Y_T and Z_T as

$$\theta = \cos^{-1}\left[\frac{Z_T}{\sqrt{X_T^2 + Y_T^2 + Z_T^2}}\right] \quad \left(0^\circ \le \theta \le 180^\circ\right) \quad (12)$$

$$\phi = \tan^{-1}\left[\frac{Y_T}{X_T}\right] \quad (13)$$

Therefore, the coordinates of P can be written in terms of the coordinates of T as follows.

$$X_P = R\cos\left[\tan^{-1}\left(\frac{Y_T}{X_T}\right)\right] \quad (14)$$

$$Y_P = R\sin\left[\tan^{-1}\left(\frac{Y_T}{X_T}\right)\right] \quad (15)$$

$$Z_P = R\cot\left[\cos^{-1}\left(\frac{Z_T}{\sqrt{X_T^2 + Y_T^2 + Z_T^2}}\right)\right] \quad (16)$$

3.2 Distance Calculation for the Transducers and the Inner Wall of the Tube

The CWT(continuous-time wavelet transform) is especially valuable for analyzing signals which have high frequency components for short duration and low frequency components for extended periods (Vetterli and Kovacevic, 1995), therefore the method was used for estimating the distance between the transducers and the inner wall of the tube. The signal velocities in low alloy steel and water are 3150 m/s and 1480 m/s respectively which means the speed of ultrasound in tube is higher than in water. It is known apriori that 0.047 inches corresponds to 63 pixels in the B-scan. This corresponds to the thickness of the tube wall. The time required for the wave to traverse 0.047 inches in water can be obtained using Snell's law (Schmerr, 1998),

$$\frac{T_M}{T_W} = \frac{V_W}{V_M} = \frac{1}{\varepsilon} = \frac{\sin 19.5^\circ}{\sin 45^\circ} = 0.4721 \quad (17)$$

where T_M, T_W is the time in metal and water, V_M, V_W is the velocity in metal and water and the ε is the relative index of refraction respectively. From the Snell's law in eqn. (17), $T_W = T_M \times \varepsilon$, therefore, the distance corresponding to 63 time pixels in metal, which is known to correspond to the thickness of the tube (0.047 inches), is the same as 63ε time pixels in water from the B-scan image where $\varepsilon = 2.1183$. Table I shows the distances in water and metal for one pixel. It can be noticed that the signal's travel velocity in metal is approximately twice faster than that in water.

Therefore, 0.000352192 is multiplied with the measured TOF to obtain the distance in inches. The angle of incidence should also be considered to calculate the shortest distance from the transducer to the ID (inner diameter). The incident angle is 19.5° consequently we need to multiply cos19.5° with the measured distance to compute a shortest distance.

Table 1 Distance for one pixel in metal and water

	In Metal	In Water
0.047 inch	63 pixels (known)	63ε pixels
One pixel	0.000746 inch	0.000352192 inch

4. MSE Minimization Using the LMS Algorithm

The gradient of mean square error (MSE) is employed to estimate the canting angle as well as C_x and C_y. The angle ϕ cannot be estimated from the data due to rotational symmetry. The sum of all the distances between the probe and the tube wall can be estimated from the B-scan image. However the data does not contain any information to estimate ϕ. Although the direction of Z-axis can be fixed, the X, Y axis cannot be fixed to allow estimation of ϕ. In addition, C_z does not need to be estimated since we are not interested in estimating the axial position of the probe. We are therefore interested in computing the gradient with respect to θ, C_x and C_y only. The steepest descent algorithm can be considered as an efficient gradient type method because it works with the true gradient vector, and not with an estimate. Therefore the performance of other gradient type algorithms can at most be close to the performance of the steepest descent method (Solo and Kong, 1995). Using this iterative minimization procedure, the optimum value for θ, C_x and C_y which give the minimum error can be achieved by orienting the search in a direction that is opposite to that of the gradient of E.

5. Classification Using SAFT and Centroid Technology

Synthetic aperture focusing techniques (SAFT) process data so as to simulate a larger transducer to obtain better resolution and signal to noise ratio (SNR) (Masri et al., 1994). A-scan signals are first time-shifted in order to align the reflections from scatterers. The time-shifted signals are then added up coherently so that the point of focus coincides resulting in the reconstruction of an image with improved SNR. Usually the ultrasonic backscattered echoes are corrupted randomly by noise from different sources. In order to minimize the noise, the average can be computed from the processed signal after many signals are taken at the same location. The resulting signal contains a lower level of noise since noise contained in each of the signals are not correlated. In contrast, signals generated due to discontinuities in the materials are added coherently resulting in an improvement in SNR. The SAFT uses the same concept using many A-scans obtained at different locations. Many shape features can be conveniently represented in terms of moments. The spatial moment concept is applied to images by forming spatial summations over a image function $I(x,y)$. The location of the centroid of the scatterer with respect to the tube wall can be used as a basis for determining if the scatterer is a crack located within the tube wall or is due to ihnomogeneity in the deposit. The centroid, called the center of gravity, is the balance point of the image function $I(x,y)$ such that the mass of the left and right of $\bar{x}$ and above and below $\bar{y}$ is equal. Let $I \in R^2$ be an image that represents an object consisting of positive-valued pixels that is set against a background of 0-valued pixels where R stands for the two dimensional space. Position refers to the location of the object in the plane. The object's centroid (or center of mass) is the point that is used to specify its position. The centroid is the point $(\bar{x}, \bar{y})$ whose coordinates are given by

$$\bar{x} = \frac{\int\int_{R^2} x \cdot I(x,y)dxdy}{\int\int_{R^2} I(x,y)dxdy} \quad (18)$$

$$\bar{y} = \frac{\int\int_{R^2} y \cdot I(x,y)dxdy}{\int\int_{R^2} I(x,y)dxdy} \quad (19)$$

For digital image $I \in R^{Z_m \times Z_n}$ the centroid's coordinates are given by

$$\bar{x} = \frac{\sum_{x=1}^{m}\sum_{y=1}^{n} x \cdot I(x,y)}{\sum_{x=1}^{m}\sum_{y=1}^{n} I(x,y)} \quad (20)$$

$$\bar{y} = \frac{\sum_{x=1}^{m}\sum_{y=1}^{n} y \cdot I(x,y)}{\sum_{x=1}^{m}\sum_{y=1}^{n} I(x,y)} \quad (21)$$

The centroid coordinates are plotted in the reconstructed images which are obtained after the application of the SAFT.

6. Results of Classification

The estimated values of C_x, C_y and θ are used in SAFT. The value of θ allows computation of the true angle of incidence from the transducer and the beam spread angle at the tube wall at each axial position inside the tube. Figs. 4 through 9 show the images obtained after processing for cracks and deposits. In all these figures, (a) represents the input B-scan image while (b) represents the reconstructed image obtained using SAFT. In each of the Fig. 4(b) to 9(b), the reconstructed image is displayed such that the ID of the tube is the left edge of the image. This allows a closer look of the flaw. The X-axis and Y-axis of the Figs. 4(b) to 9(b) stand for steam generator tube's axial direction and cross direction respectively and the white vertical lines located at 1 and 50 on the X-axis indicate the positions of ID and OD (outer diameter) of the tube respectively. The elliptical-shaped spots in Figs. 4(b) to 9(b) indicate the locations of flaws of interest and the centroid's coordinates of the flaw image are marked with an 'X'.

Figs. 4, 5 and 7, 8 show results obtained from a straight section of the tube. For Figs. 4(b), 5(b), the flaw part is located mainly inside the OD. Consequently those are classified as cracks in the tube. In Figs. 7(b), 8(b), the flaw is located generally outside the OD and consequently those are classified as deposits. It can be noticed that the centroid's coordinates of a relatively small sized scatterer is nearly located at OD. These SAFT results do not offer significant improvement from the results obtained without the estimate of the beam spread angle since the probe is located in a straight section of the tube. Figs. 6 and 9 show results obtained from a bent section of the tube. The centroid coordinate values are listed in Tables 2 and 3

Table 2 Centroid coordinates for reconstructed images of cracks

Crack size	$\bar{x}$	$\bar{y}$
68%	33	143
47%	33	121
15%	38	115
20%	40	121
18%	41	93
31%	33	97
29%	34	108
54%	27	99
11%	37	143
20%	29	149

Table 3 Centroid coordinates for reconstructed images of deposits

Deposit size	$\bar{x}$	$\bar{y}$
45%	60	166
40%	56	124
18%	52	172
8%	51	100
10%	60	108
17%	62	105
29%	65	157
45%	102	157
33%	68	141
38%	72	145

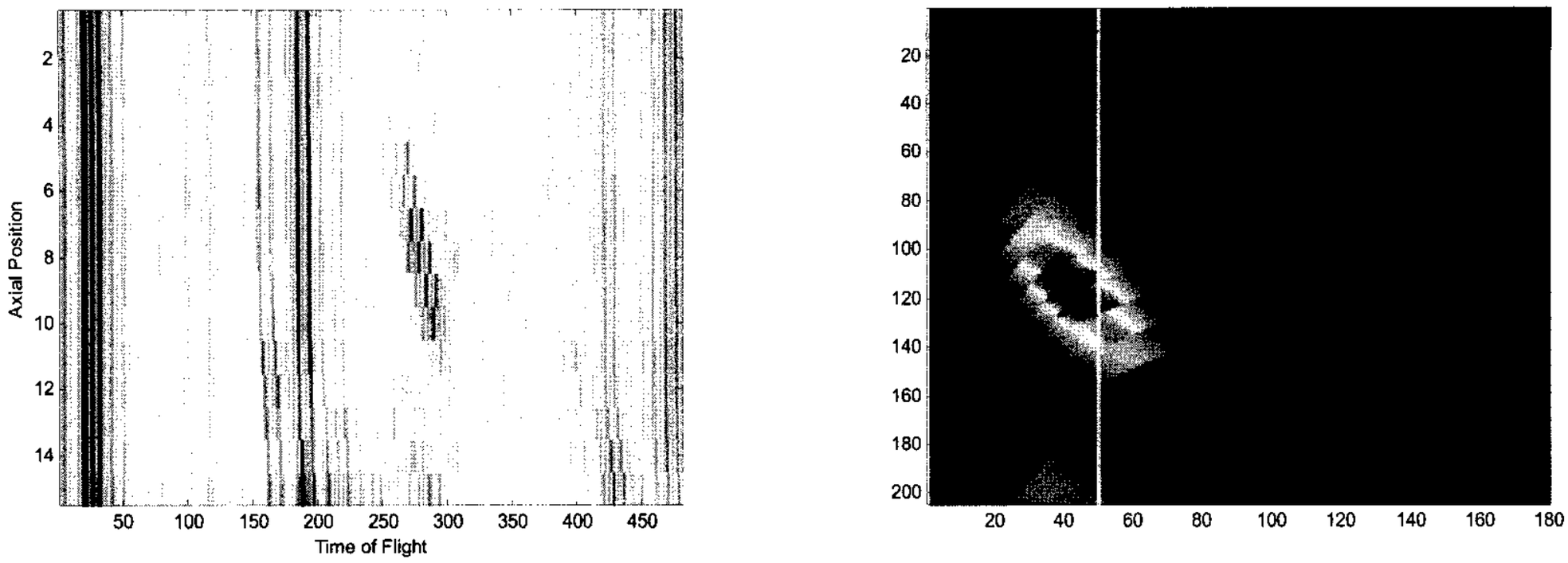

(a) (b)

Fig. 4 Input image of UT NDE and SAFT result : (a) 15% crack, (b) SAFT result for (a) in a straight section(The flaw is located inside the OD and it is classified as a crack.)

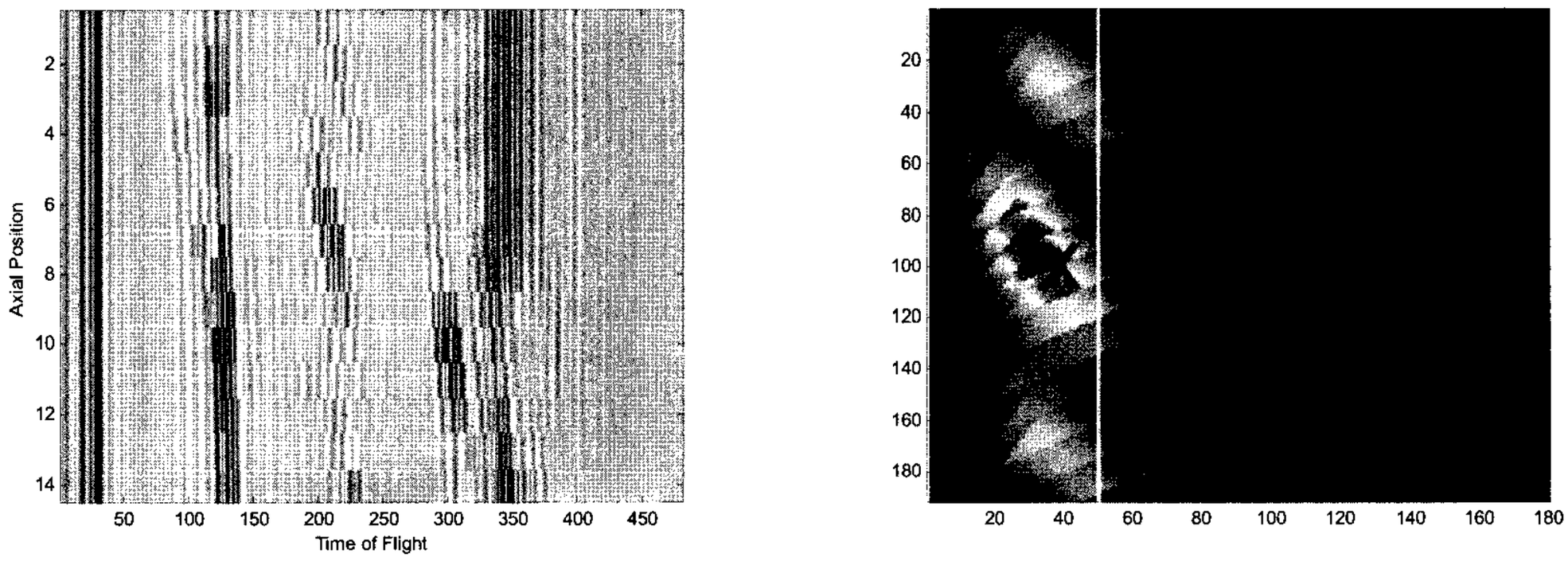

(a) (b)

Fig. 5 Input image of UT NDE and SAFT result : (a) 31% crack, (b) SAFT result for (a) in a straight section(The flaw is located inside the OD and it is classified as a crack.)

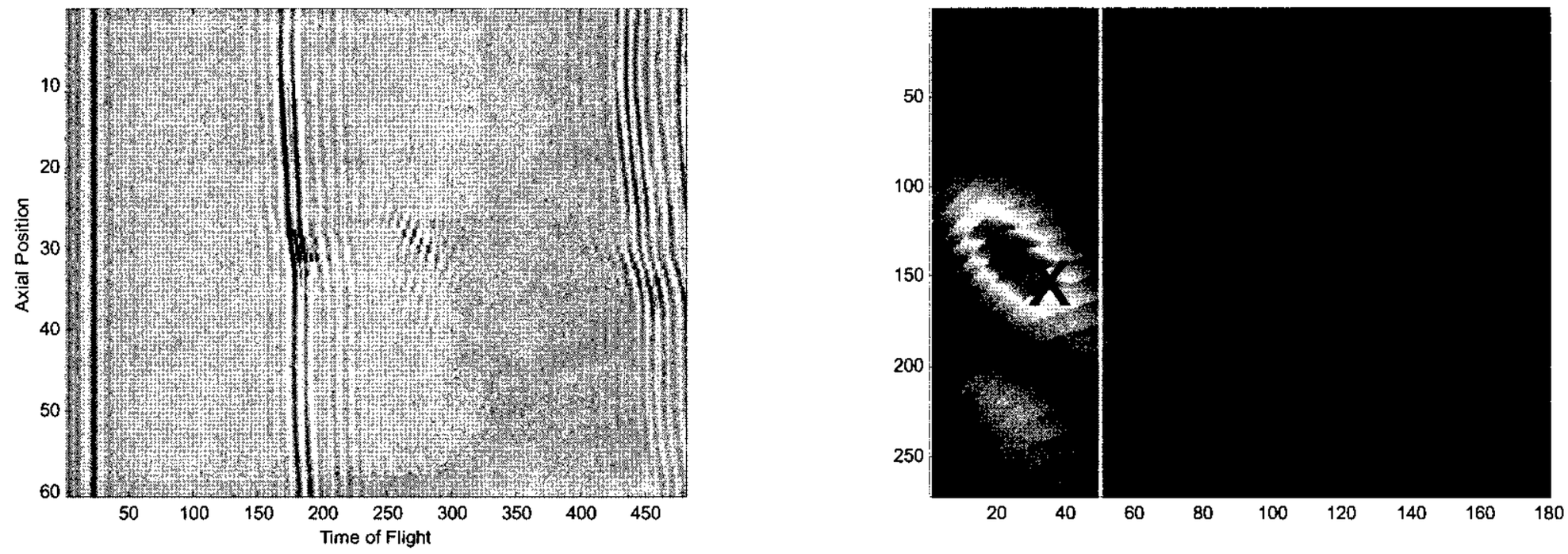

(a) (b)

Fig. 6 Input image of UT NDE and SAFT result : (a) 20% crack, (b) SAFT result for (a) in a bent section (The flaw is located inside the OD and it is classified as a crack.)

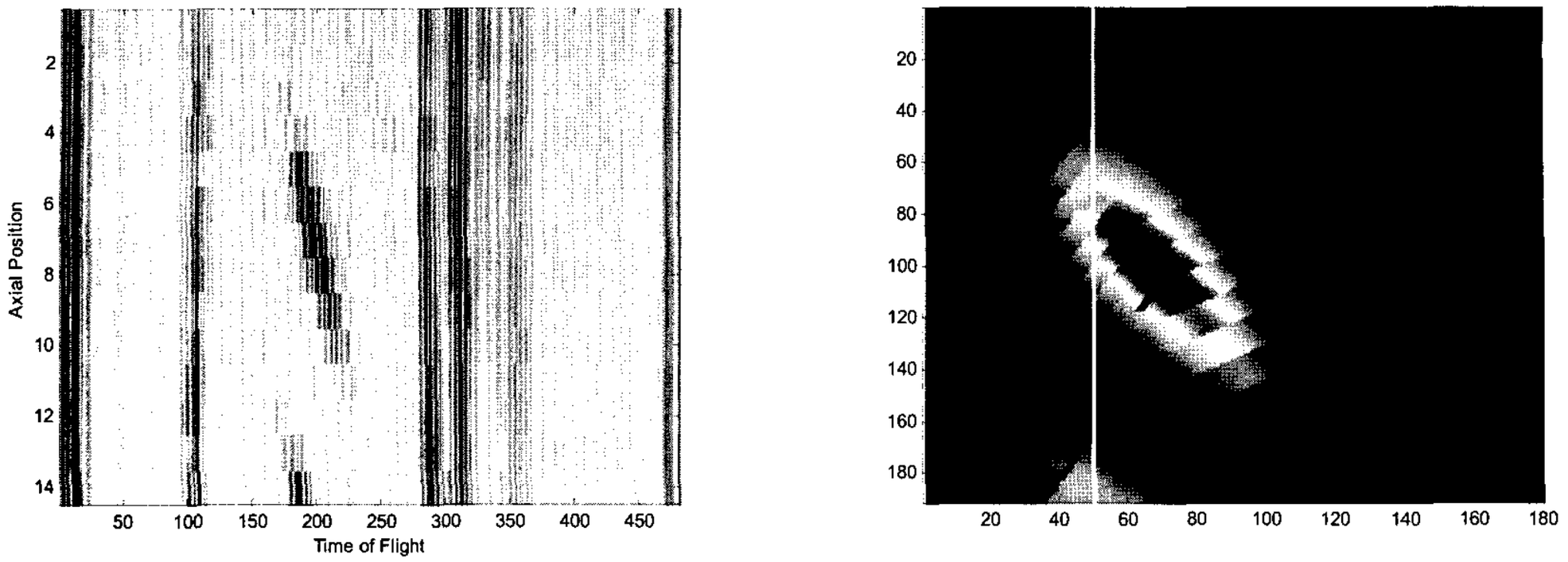

(a) (b)

Fig. 7 Input image of UT NDE and SAFT result : (a) 17% deposit, (b) SAFT result for (a) in a straight section (The flaw is located outside the OD and it is classified as a deposit.)

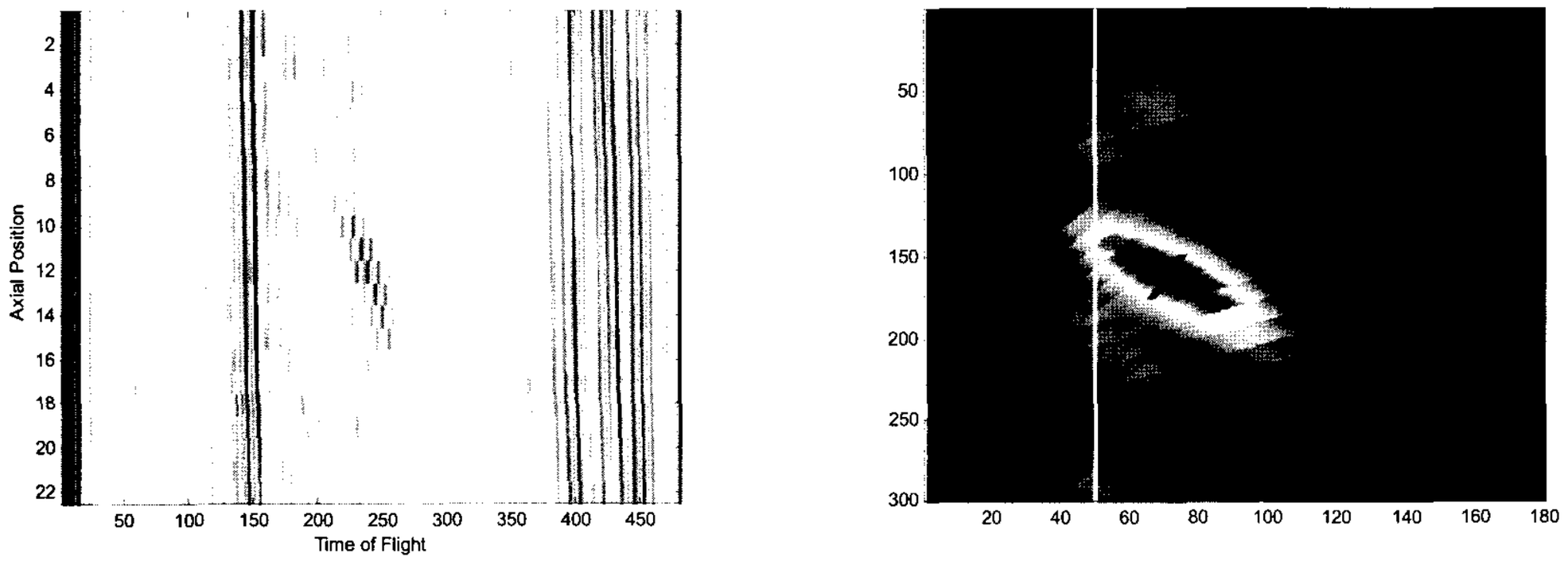

(a) (b)

Fig. 8 Input image of UT NDE and SAFT result : (a) 29% deposit, (b) SAFT result for (a) in a straight section(The flaw is located outside the OD and it is classified as a deposit.)

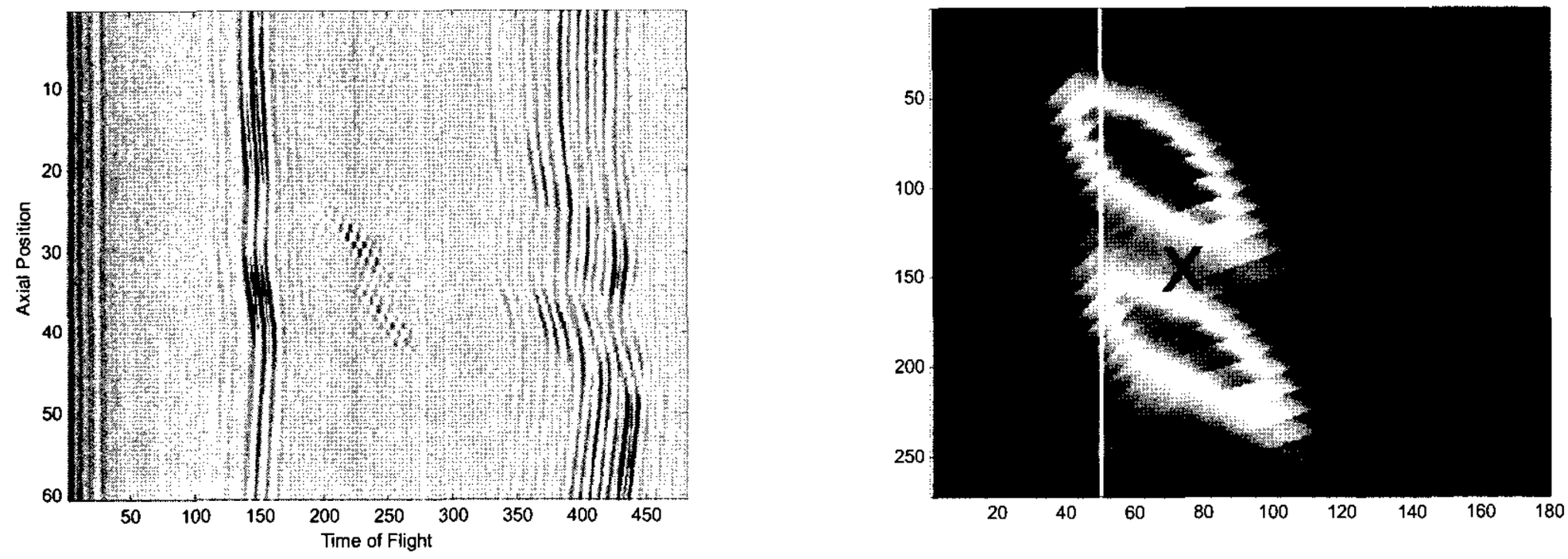

(a) (b)

Fig. 9 Input image of UT NDE and SAFT result : (a) 33% deposit, (b) SAFT result for (a) in a bent section(The flaw is located outside the OD and it is classified as a deposit.)

for cracks and deposits respectively. For Fig. 6, it appears that the flaw is mostly located between the ID and OD. Consequently it can be classified as a crack in the tube. For Fig. 9, the flaw is located outside of the OD and consequently it is classified as a deposit. The tube wall may exhibit ovality and consequently the diameter of the tube is altered. The results presented are based on the assumption that the tube is circular in a bent section.

7. Conclusion

A method for discriminating crack signals from those due to deposits for ultrasonic NDE of steam generator tubes is developed. Firstly, the characteristics of the ultrasonic signals collected are studied and a coordinate system for the probe and the tube has been developed to produce a basis for estimating the location of the transducer and the distance between those has been computed. Distance between the transducer and the tube wall from the data has been measured using CWT and consideration of the velocity effects. Expressions for gradient of the MSE with respect to the probe coordinates and canting angle have been derived and the gradient is incorporated in LMS algorithm to obtain the optimum values of probe coordinates and canting angle. The classification results show how estimates of the parameters can be used in conjunction with the SAFT and centroid technique to improve the SNR of the image and classify those defects more effectively. The classification has been performed using data from the straight and bent portions of the tube. The centroid method is used for a scatterer with respect to the tube wall so that it is used as a basis for determining more accurately if the scatterer is a crack located within the tube wall or is due to inhomogeneity in the deposit layer. The centroid's coordinates are marked in the reconstructed image to indicate the location of a scatterer with respect to the tube wall. Additional work in the future can be focused on reducing the computation time.

References

Demirli, R. and Saniie, J. (2001) Model-Based Estimation of Ultrasonic Echoes Part II:Nondestructive Evaluation Applications, *IEEE Transactions on Ultrasonics, Ferroelectrics, and Frequency Control*, Vol. 48. No. 3, pp. 803-811

Du-Yih, T. (1998) Classification of Heart Diseases in Ultrasonic Images Using Neural Networks Trained by Genetic Algorithms, *Proceedings of the Fourth International Conference on Signal Processing*, Vol. 2, pp. 1213-1216

Hayt, W. H. (1989) *Engineering Electromagnetics*, McGraw-Hill Book Company, New York, USA, pp. 125-128

Khan, A. (2001) Defect Classification for Steam Generator Tubes of a Nuclear Power Plant Using Ultrasonic Nondestructive Techniques, *M. S. Thesis*, Iowa State University, Ames, IA, USA, pp. 23-26

Masri, W., Mina, M., Udpa, S. S., Udpa, L. and Lord, W. (1994) Synthetic Aperture Focusing Technique Using the Envelope Function for Ultrasonic Imaging, *Review of Progress in Quantitative NDE*, Vol. 14A, pp. 909-914

Polikar, R., Udpa, L., Udpa, S. S. and Taylor, T. (1998) Frequency Invariant Classification of Ultrasonic Weld Inspection Signals, *IEEE Transactions on Ultrasonics, Ferroelectrics and Frequency Control*, Vol. 45, No. 3, pp. 614-625

Schmerr, L. W. Jr. (1998) *Fundamentals of Ultrasonic Nondestructive Evaluation*, Plenum Publishing Corporation, New York, USA, pp. 167-169

Solo, V. and Kong, X. (1995) *Adaptive Signal Processing Algorithms*, Prentice Hall, New York, USA, pp. 56-58

Taxt, T. (2001) Three-Dimensional Blind Deconvolution of Ultrasound Images, *IEEE Transactions on Ultrasonics, Ferroelectrics, and Frequency Control*, Vol. 48, No. 4, pp. 867-871

Vetterli, M. and Kovacevic J. (1995) *Wavelets and Subband Coding*, Prentice Hall PTR, New York, USA, pp. 78-79